

# Litmus tests of the flat $\Lambda$ CDM model and model-independent measurement of $H_0 r_d$ with LSST and DESI

Benjamin L'Huillier <sup>a</sup>, Ayan Mitra <sup>b,c</sup>, Arman Shafieloo <sup>d,e</sup>,  
Ryan E Keeley <sup>f</sup> and Hanwool Koo <sup>g</sup>

<sup>a</sup>Department of Physics and Astronomy, Sejong University, 05006 Seoul, Korea

<sup>b</sup>Center for AstroPhysical Surveys, National Center for Supercomputing Applications, University of Illinois Urbana-Champaign, Urbana, IL, 61801, USA

<sup>c</sup>Department of Astronomy, University of Illinois at Urbana-Champaign, Urbana, IL 61801, USA

<sup>d</sup>Korea Astronomy and Space Science Institute, Daejeon 34055, Korea

<sup>e</sup>University of Science and Technology, Daejeon 34113, Korea

<sup>f</sup>University of California, Merced, 5200 N Lake Road, Merced, CA 95341, USA

<sup>g</sup>Department of Physics and Astronomy, University of the Western Cape, Robert Sobukwe Road, Bellville, Cape Town, 7535, South Africa

E-mail: [benjamin@sejong.ac.kr](mailto:benjamin@sejong.ac.kr), [ayan@illinois.edu](mailto:ayan@illinois.edu), [shafieloo@kasi.re.kr](mailto:shafieloo@kasi.re.kr),  
[rkeeley@ucmerced.edu](mailto:rkeeley@ucmerced.edu), [hanwool.koo90@gmail.com](mailto:hanwool.koo90@gmail.com)

**Abstract.** In this analysis we apply a model-independent framework to test the flat  $\Lambda$ CDM cosmology using simulated SNIa data from the upcoming Large Synoptic Survey Telescope (LSST) and combined with simulated Dark Energy Spectroscopic Instrument (DESI) five-years Baryon Acoustic Oscillations (BAO) data. We adopt an iterative smoothing technique to reconstruct the expansion history from SNIa data, which, when combined with BAO measurements, facilitates a comprehensive test of the Universe's curvature and the nature of dark energy. The analysis is conducted under three different mock true cosmologies: a flat  $\Lambda$ CDM universe, a universe with a notable curvature ( $\Omega_{k,0} = 0.1$ ), and one with dynamically evolving dark energy. Each cosmology demonstrates different kinds and varying degrees of deviation from the standard model predictions. We forecast that our reconstruction technique can constrain cosmological parameters, such as the curvature ( $\Omega_{k,0}$ ) and  $H_0 r_d$ , with a precision of approximately 0.52% for  $H_0 r_d$  and between 0.032 to 0.037 for  $\Omega_{k,0}$ , competitive with current cosmic microwave background constraints, without assuming any form of dark energy.

---

## Contents

<b>1</b>	<b>Introduction</b>	<b>1</b>
<b>2</b>	<b>Data</b>	<b>2</b>
2.1	Fiducial Models	2
2.2	LSST SNIa Simulations	3
2.2.1	Vera C. Rubin Observatory (The LSST)	3
2.2.2	Mock Data Generation	3
2.3	Mock BAO data from DESI 5-year	4
<b>3</b>	<b>Method</b>	<b>5</b>
3.1	Curvature test	6
3.2	Iterative Smoothing	7
<b>4</b>	<b>Results</b>	<b>10</b>
4.1	Supernova Smoothing	10
4.2	$H_0 r_d$	11
4.3	Curvature Test	14
<b>5</b>	<b>Summary and Conclusion</b>	<b>14</b>
<b>A</b>	<b>Smooth Derivatives</b>	<b>14</b>

---

## 1 Introduction

The concordance cosmological  $\Lambda$ CDM model relies on a few assumptions. Among them, homogeneity and isotropy lead to the Friedman-Robertson-Lemaître-Walker (FLRW) metric. The discovery of cosmic acceleration led to the establishment of the concordance  $\Lambda$ CDM model. In this model, the energy budget of the Universe is dominated by a cosmological constant  $\Lambda$ , and matter by cold dark matter (CDM). The most stringent constraints on the model have been obtained by cosmic microwave background (CMB) measurements from the Planck satellite [1], baryon acoustic oscillations (BAO) [2–6] and Type Ia Supernovae (SNIa) [7–11]. CMB constrains the curvature parameter to be  $\Omega_k = -0.044^{+0.018}_{-0.015}$ . Most of these constraints however are direct fits to the data assuming a particular model, typically the  $\Lambda$ CDM model or an extension. While this leverages the power of Bayesian statistics to provide tight constraints on the model parameters, it is important to also test the validity of the underlying hypotheses.

As opposed to model-fitting, model-independent approaches provide a healthy check on the validity of a given model. Due to their extra flexibility compared to model-fitting approaches, they may also reveal the presence of unexpected features in the data and may be used to look for unaccounted for systematics [12–14].

The rise of tensions, in particular the Hubble tension, and the unknown nature of the main components of the model are strong hints for cosmologist to search for evidence for beyond- $\Lambda$ CDM physics [15–23].

Recent data from the Dark Energy Spectroscopic Instrument (DESI) showed evidence for a phantom dark energy or a dynamical dark energy [5]. This was further confirmed by

studying physics-driven modifications of  $\Lambda$ CDM [24] as well as data-driven reconstructions of the expansion history [25].

The curvature of the Universe is another fundamental question. The Planck 2018 data are consistent with a flat universe but do not exclude a small negative curvature [1], see also [26]. DESI DR1 finds a preference for a small positive curvature, which disappears when combined with Planck.

In this work, we used a model-independent approach, namely, the iterative smoothing method, to reconstruct the expansion history from SNIa and combine it with distance measurements from BAO to perform a litmus test of the pillars of the  $\Lambda$ CDM model, the FLRW metric, the flatness of the Universe, and the cosmological constant, as well to constrain  $H_0 r_d/c$ .

## 2 Data

In this analysis, we used simulated 3-year LSST<sup>1</sup> SNIa data and the BAO forecast for DESI from [27] to constrain cosmology.

### 2.1 Fiducial Models

To show the potential of our model-independent approach, we simulate data for three different cosmologies:

- a flat- $\Lambda$ CDM universe, with  $\Omega_{m,0} = 0.315$  and a constant equation of state  $w = -1$ .
- a curved  $\Lambda$ CDM universe, with  $(\Omega_{m,0}, \Omega_{k,0}) = (0.315, 0.1)$ . While such a large curvature is consistent with Pantheon+ or DESI DR1 data, it is excluded by Planck 2018 data. However, it is nonetheless interesting to see the effect of curvature and to apply our curvature test to a curved universe.
- a flat universe with dynamical dark energy. We chose the phenomenologically emergent dark energy (PEDE) model [28], which has no extra degree of freedom relative to  $\Lambda$ CDM. The dark energy density evolves as

$$f_{\text{PEDE}}(z) = 1 - \tanh(\log_{10}(1+z)) \quad (2.1a)$$

and the equation of state

$$w_{\text{PEDE}}(z) = \frac{1}{3 \ln 10} (1 + \tanh[\log_{10}(1+z)]) - 1 \quad (2.1b)$$

We note that the data and covariance matrix were initially generated for the flat  $\Lambda$ CDM case, and we reused the same noise and covariance matrix for the other two cosmologies. While for a proper forecast, one should apply the pipeline from [29] using the other two fiducial cosmologies, we assume here that the resulting noise and covariance should be affected minimally by the change of fiducial cosmology. On the other hand, the mock BAO data are all generated with Gaussian white noise.

Table 1 summarizes our three fiducial cosmologies.

---

<sup>1</sup>[www.lsst.org](http://www.lsst.org)

Fiducial Cosmology	$\Omega_{m,0}$	$h$	$\Omega_{k,0}$	$w$
flat- $\Lambda$ CDM	0.315	0.685	0	-1
$\Omega_{k,0} = 0.1$	0.315	0.685	0.1	-1
PEDE	0.315	0.685	0	Eq. (2.1b)

**Table 1:** Fiducial cosmologies used in this work

## 2.2 LSST SNIa Simulations

### 2.2.1 Vera C. Rubin Observatory (The LSST)

The forthcoming LSST survey, scheduled to commence in 2025, represents the most comprehensive optical survey planned to date, marking a significant milestone for its generation. This survey will run for a decade and will extensively explore the southern hemisphere’s sky through a large, ground-based, wide-field observatory utilising six optical passband filters. This combination is designed to achieve an unparalleled balance of depth, coverage area, and observational frequency. Over the course of the survey, the *LSST* is expected to catalogue millions of supernovae [30]. Operating from the Rubin Observatory, the Simonyi Survey Telescope features an 8.4 m mirror (with an effective aperture of 6.7 m) and is equipped with a state-of-the-art 3200-megapixel camera, providing a 9.6 deg<sup>2</sup> field of view. Approximately 90% of the telescope’s time will be dedicated to a deep-wide-fast survey mode, systematically covering an area of 18,000 square degrees roughly 800 times across all bands over a decade, resulting in a co-added map with a depth of  $r - 27.5$  (called as the Wide Fast Deep (WFD) observing strategy in the LSST). This extensive data collection is projected to amass around 32 trillion observations of 20 billion galaxies and an equivalent number of stars, primarily supporting the survey’s main scientific objectives [30]. The remaining 10% of the time will be reserved for specific initiatives, such as the Very Deep and Very Fast time-domain surveys<sup>2</sup>, which are still in the planning stages.

### 2.2.2 Mock Data Generation

This study employs simulated SNIa data to examine dark energy results from the forthcoming LSST observations, as detailed in [29]. The supernova data are generated through the LSST Dark Energy Science Collaboration (DESC) Time Domain (TD) pipeline and the *SNANA* software [31]. The procedure encompasses four primary stages, depicted in Figure 4 of [29].

The simulations utilise the flat  $\Lambda$ CDM model from § 2.1. In particular, the Hubble constant,  $H_0$ , is set at 70.0 km s<sup>-1</sup>Mpc<sup>-1</sup>, aligned with the SALT2 model training. The SALT2 light curve model is employed to derive observer frame magnitudes. The simulation noise is calculated using the following equation:

$$\sigma_{\text{SIM}}^2 = [F^2 + (A \cdot b)^2 + (F \cdot \sigma_{\text{ZPT}})^2 + \sigma_0 \cdot 10^{0.4 \cdot ZPT_{\text{pc}}} + \sigma_{\text{host}}^2] S_{\text{SNR}}^2. \quad (2.2)$$

where  $F$  represents the simulated flux in photoelectrons,  $A$  denotes the noise equivalent area, given by  $A = [2\pi \int \text{PSF}^2(r, \theta) r dr]^{-1}$ , with PSF standing for the Point Spread Function, and  $b$  represents the background per unit area (inclusive of sky, CCD readouts, and dark current). The scale factor  $S_{\text{SNR}}$  is empirically determined based on the signal-to-noise ratio. The terms represented by  $\sigma$  denote uncertainties related to zero point, flux calibration, and

<sup>2</sup>Deep Drilling Fields (DDF)

the underlying host galaxy, empirically fitted to match simulated uncertainties with those derived from the survey designs.

The LSST TD pipeline involves SN brightness standardisation via a Light Curve (LC) fit stage, simulations for bias correction, and a BEAMS with Bias Corrections (BBC) stage for Hubble diagram production. This pipeline yields a redshift-binned Hubble diagram and its associated covariance matrix, which are the data products employed for cosmological fitting.

The SNIa dataset utilised comprises both spectroscopically ( $z_{\text{spec}}$ ) and photometrically ( $z_{\text{phot}}$ ) identified SNIa candidates. Based on PLAsTiCC [32], the “ $z_{\text{spec}}$ ” sample includes two sets of events with spectroscopic redshifts featuring an accuracy of  $\sigma_z \sim 10^{-5}$ . The first subset consists of spectroscopically confirmed events with accurate redshift predictions by the 4MOST spectrograph [33], under construction by the European Southern Observatory and expected to be operational in 2024, situated at a latitude similar to that of the Rubin Observatory in Chile. The second subset includes photometrically identified events with accurate host galaxy redshifts determined by 4MOST, with this subset being approximately 60% larger than the first. For the photometric sample, host galaxy photometric redshifts were employed as priors (adapted from [34]). The photometric redshift and rms uncertainty derive from [35]. The entire simulation was rerun based on the PLAsTiCC DDF data<sup>3</sup>. Additional low redshift spectroscopic data was sourced from the DC2 analysis, simulated with WFD cadence. [29] restricted simulations to SNIa, omitting contamination (*e.g.* core collapse, peculiar SNe, *etc.*). The covariance matrix corresponds to the combined statistical and systematic errors, where the latter encompasses all individual systematics, detailed in Table 3 of [29]. The Hubble diagram is segmented into 14 redshift bins, containing a total of 5809 SNIa candidates, both spectroscopic and photometric.

It is noteworthy that [29] introduce a dataset with characteristics akin to those projected in the LSST science roadmap for 1 and 10 years of SNIa cosmology analysis, as described by [36]. However, there are significant differences. While the analysis by [36] relies solely on SNIa with spectroscopically confirmed host redshifts, [29] broadens the scope by including a comprehensive end-to-end analysis that incorporates both spectroscopic and photometric redshifts of host galaxies. In the forthcoming LSST era, it is anticipated that the volume of photometrically observed Type Ia supernovae will vastly outnumber the spectroscopic candidates. The methodology presented in [29] therefore enables the use of these photometric candidates in the cosmology analysis and hence in construction of a denser Hubble diagram with higher redshift reaches. As a result, this presents a critical opportunity to leverage photometric supernovae in cosmological analyses, and potentially amplifying the dark energy constraints significantly.

### 2.3 Mock BAO data from DESI 5-year

The Dark Energy Spectroscopic Instrument (DESI) is a stage-IV experiment aiming to constrain dark energy by mapping the Universe in three dimensions [6].

BAO are another probe of the expansion history from large-scale structures. Strictly

---

<sup>3</sup>The LSST utilises different observing strategies, namely the deep field and the wide field, termed the DDF (Deep Drilling Field) and the WFD (Wide Fast Deep), respectively.

speaking, the transverse and radial modes of the BAO constrain

$$\frac{d_A(z)}{r_d} = \frac{c}{H_0 r_d} \frac{\mathcal{D}(z)}{1+z}, \text{ and} \quad (2.3a)$$

$$\frac{c}{H(z)r_d} = \frac{c}{H_0 r_d} \frac{1}{h(z)}, \quad (2.3b)$$

where

$$\frac{H_0 r_d}{c} = \frac{1}{\sqrt{3}} \int_0^{\frac{1}{1+z_d}} \frac{da}{a^2 h(a) \sqrt{1 + \frac{3\omega_b}{4\omega_\gamma} a}} \quad (2.3c)$$

and  $r_d$  is the sound horizon at the drag epoch  $z_d$ .

We generated DESI 5-year mock BAO, assuming a Gaussian white noise where the errors are taken from [27]. While for real data, one must take care of the correlation between  $d_A$  and  $c/Hr_d$ , in this paper we assume that there is no correlation. We also assume  $H_0 = 70 \text{ km s}^{-1} \text{ Mpc}^{-1}$ , and  $r_d = 147.10 \text{ Mpc}$ , leading to a fiducial value  $H_0 r_d^{\text{fid}} = 10\,297 \text{ km s}^{-1} \text{ Mpc}^{-1} = 0.03435 c$ . While such cosmology is not currently favored by CMB experiments, the exact choice of cosmological parameters is not important for the purpose of this study since we are focusing on model independent reconstructions and so our results do not depend on different fiducial models.

### 3 Method

In an FLRW universe, when radiation is negligible, the expansion history reads

$$h^2(z) = \frac{H^2(z)}{H_0^2} = \Omega_{m,0}(1+z)^3 + \Omega_{k,0}(1+z)^2 + (1 - \Omega_{m,0} - \Omega_{k,0})f_{\text{DE}}(z), \quad (3.1a)$$

where

$$f_{\text{DE}}(z) = \exp\left(3 \int_0^z \frac{1+w(x)}{1+x} dx\right) \quad (3.1b)$$

describe the time evolution of the dark energy density,  $\Omega_{m,0}$  and  $\Omega_{k,0}$  are the matter and curvature density parameters today respectively, and  $w = p/\rho$  is the equation of state of dark energy. For the cosmological constant  $\Lambda$ ,  $w = -1$  and  $f_{\text{DE}}(z) \equiv 1$ .

The dimensionless comoving distance is defined by

$$\mathcal{D}(z) = \frac{1}{\sqrt{-\Omega_{k,0}}} \sin\left[\sqrt{-\Omega_{k,0}} \int_0^z \frac{dx}{h(x)}\right] \quad (3.2)$$

for all signs of  $\Omega_{k,0}$ . In particular, for  $\Omega_{k,0} = 0$ , eq. (3.2) simplifies to

$$\mathcal{D}(z) = \int_0^z \frac{dx}{h(x)}. \quad (3.3)$$

The angular diameter and luminosity distances are related to the comoving distance by

$$(1+z)d_A(z) = \frac{d_L(z)}{1+z} = d_C(z) = \frac{c}{H_0} \mathcal{D}(z). \quad (3.4)$$

The distance modulus from supernovae is

$$\mu(z) = 5 \log_{10} \frac{d_L}{1 \text{ Mpc}} + 25. \quad (3.5)$$

Several litmus tests have been put forward to test various aspects of the  $\Lambda$ CDM model. In particular, in an FLRW universe, we have [37–39]

$$\mathcal{O}_k(z) = \frac{\Theta^2(z) - 1}{\mathcal{D}^2(z)} = \Omega_{k,0}, \quad (3.6a)$$

where

$$\Theta = h\mathcal{D}'. \quad (3.6b)$$

In a flat-FLRW universe,  $\Theta(z) \equiv 1$ .

The  $O_m$  diagnostic, introduced by [40], is defined as

$$O_m(z) = \frac{h^2(z) - 1}{(1+z)^3 - 1} = \Omega_{m,0} \quad (3.7)$$

in a flat- $\Lambda$ CDM universe. These two diagnostics are litmus tests respectively of the FLRW metric (and its curvature) and of the flat- $\Lambda$ CDM model. Departure from  $O_m = \text{constant}$ , or from  $\mathcal{O}_k = \text{constant}$  are signs of departure from flat- $\Lambda$ CDM and FLRW respectively.

Another widely used quantity is the deceleration parameter

$$q = -\frac{1}{H} \frac{\ddot{a}}{a} = -(1+z) \frac{h'}{h} - 1. \quad (3.8)$$

$q > 0$  indicate a decelerating Universe, while  $q < 0$  for an accelerating universe.

### 3.1 Curvature test

The transverse and radial BAO modes respectively give us  $d_A/r_d = d_C/((1+z)r_d)$  and  $c/(Hr_d)$ , while the supernovae provide  $\mathcal{D}$  and  $\mathcal{D}'$ , which are independent of both  $H_0$  and  $r_d$ . We can therefore combine these two measurements to estimate  $H_0 r_d$  in two independent ways:

$$\frac{H_0 r_d}{c} = \mathcal{D} \frac{r_d}{d_C}, \text{ and} \quad (3.9a)$$

$$\frac{H_0 r_d}{c} = \frac{1}{h} \frac{H r_d}{c} = \mathcal{D}' \frac{H r_d}{c}, \quad (3.9b)$$

where the last equality holds only for a flat-FLRW universe. Therefore, we can combine the BAO observables with  $\mathcal{D}$  and  $\mathcal{D}'$  measured by SNIa to constrain  $H_0 r_d$ . One way to do this is to reconstruct a smooth comoving distance  $\mathcal{D}(z)$ , its derivative  $\mathcal{D}'(z)$ , and expansion history  $h(z)$  from SNIa at any arbitrary redshift  $z$ , and evaluate those curves at the BAO redshifts  $z_{\text{BAO}}$ . To do the reconstructions, we apply the iterative smoothing method to simulated LSST SNIa as described in Section 3.2. We then simply divide the central value of the BAO measurements  $d_C/r_d$  and  $d_H/r_d$  by the value of the reconstructed  $\mathcal{D}(z_{\text{BAO}})$ ,  $\mathcal{D}'(z_{\text{BAO}})$ , and  $h(z_{\text{BAO}})$ , and then propagate the BAO error. The results of this calculation are seen in Fig. 4.

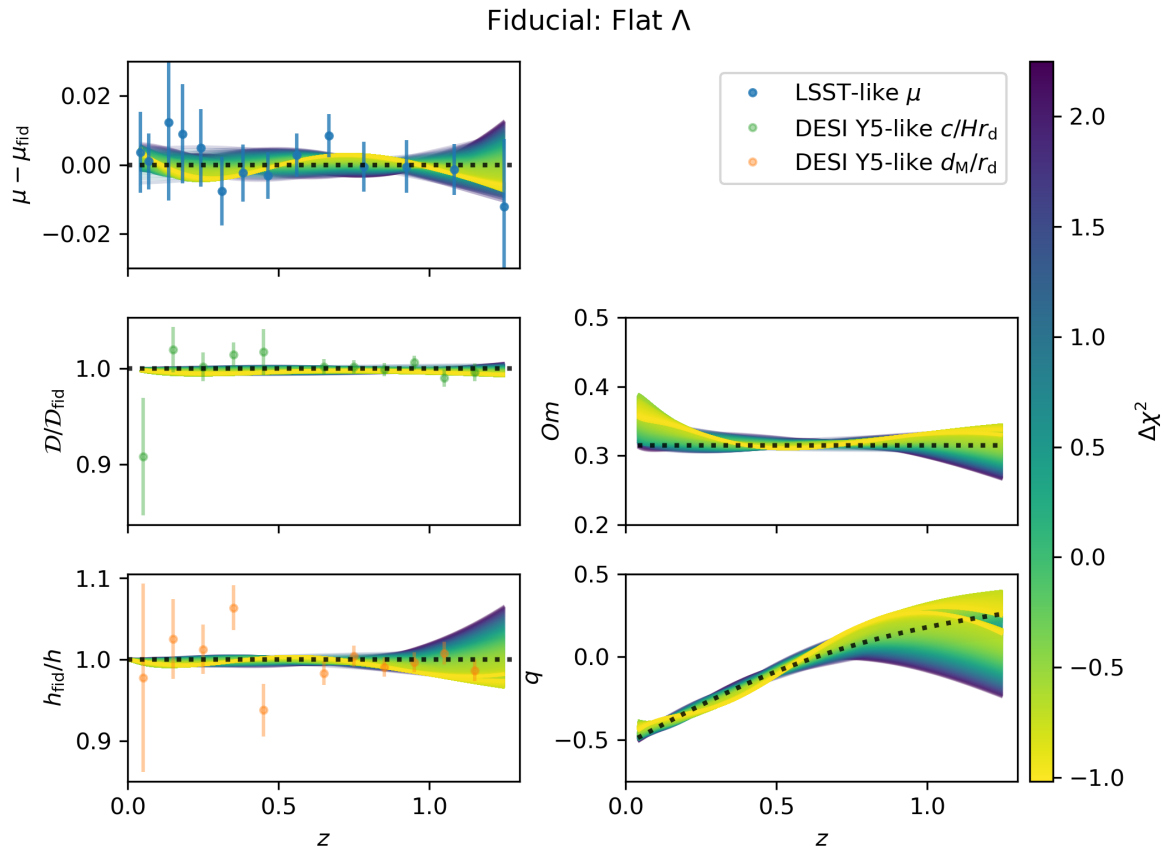


**Figure 1:** Results of the SNIa smoothing colour-coded by  $\Delta\chi^2 = \chi^2 - \chi_{\Lambda\text{CDM}}^2$  for the flat- $\Lambda$ CDM fiducial cosmology. The top-left panel shows the smooth residuals. The middle-left panel shows  $D/D_{\text{fid}}$ , the bottom-left panel shows  $h_{\text{fid}}/h$ , the middle-right panel shows  $Om$ , and the bottom-right panel  $q$ . The middle- and bottom-left panels also show the DESI-like BAO mock data normalized by the fiducial cosmology.

We can then calculate

$$\Theta = h\mathcal{D}' = \frac{Hr_d}{H_0r_d}\mathcal{D}' = \frac{Hr_d}{c} \frac{d_C}{r_d} \frac{\mathcal{D}'}{\mathcal{D}} \quad (3.10)$$

and  $\mathcal{O}_k$  only with the BAO and the smooth reconstructions from the SNIa data. Similarly to  $H_0r_d$ , we evaluate  $\Theta(z)$  by multiplying the central values of the BAO data ( $\frac{Hr_d}{c}$  and  $\frac{d_C}{r_d}$ ) with the smooth functions reconstructed from the SNIa ( $\frac{\mathcal{D}'(z_{\text{BAO}})}{\mathcal{D}(z_{\text{BAO}})}$ ), evaluated at the BAO redshifts.

### 3.2 Iterative Smoothing

We used the iterative smoothing method to reconstruct the distance-redshift relation from SNIa [41–43]. The strength of this method is that we make no assumption regarding the evolution of dark energy.

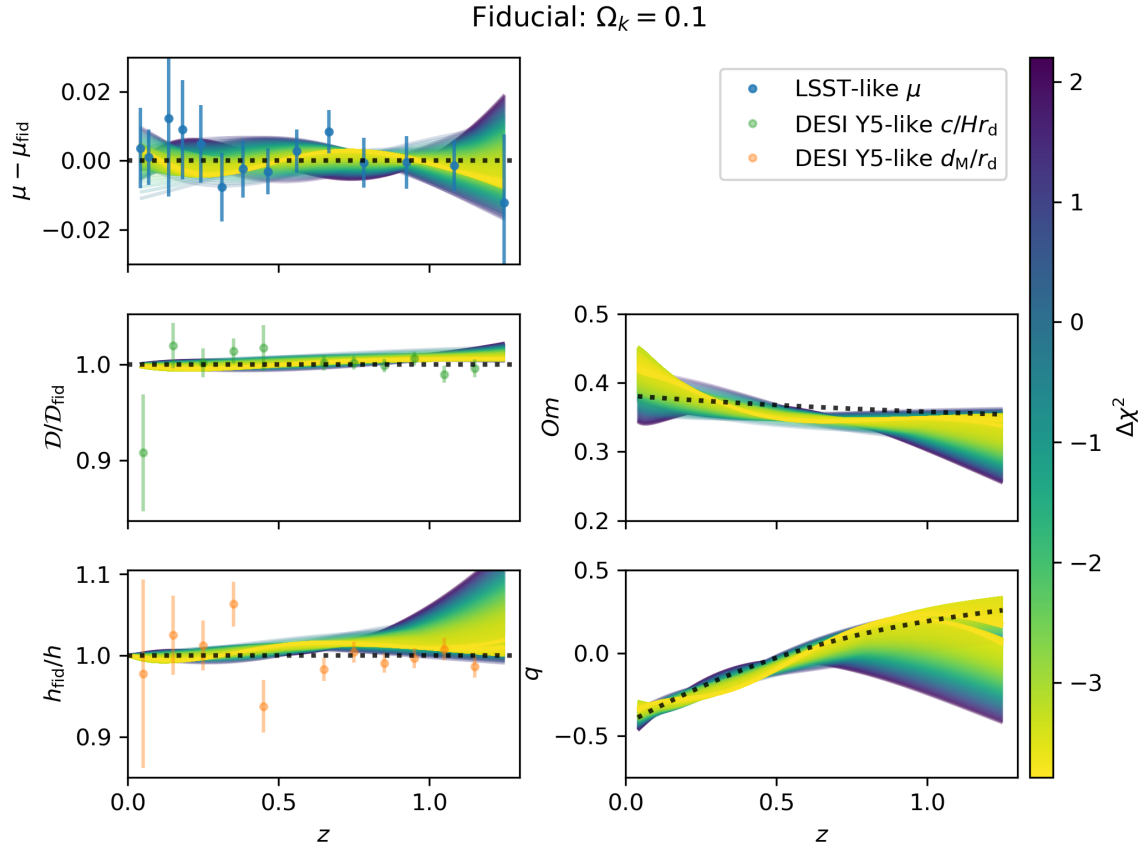


**Figure 2:** Same as Fig. 1, fiducial model:  $\Lambda$ CDM ( $\Omega_{k,0} = 0.1$ ) Note that in the bottom-left panel, the BAO data are  $h_{\text{fid}}/h$ , but the smooth SNIa reconstructions show  $\mathcal{D}'/\mathcal{D}'_{\text{fid}}$ .

Starting with some initial guess  $\hat{\mu}_0$ , we iteratively calculate the reconstructed  $\hat{\mu}_n + 1$  at iteration  $n + 1$  with the inverse covariance matrix of the SNIa data  $\mathbf{C}_{\text{SN}}^{-1}$ :

$$\hat{\mu}_{n+1}(z) = \hat{\mu}_n(z) + \frac{\delta\boldsymbol{\mu}_n^\top \cdot \mathbf{C}_{\text{SN}}^{-1} \cdot \mathbf{W}(z)}{\mathbb{1}^\top \cdot \mathbf{C}_{\text{SN}}^{-1} \cdot \mathbf{W}(z)}, \quad (3.11a)$$

where

$$\mathbf{W}_i(z) = \exp\left(-\frac{\ln^2\left(\frac{1+z}{1+z_i}\right)}{2\Delta^2}\right) \quad (3.11b)$$

is a vector of weights,

$$\mathbb{1} = (1, \dots, 1)^\top \quad (3.11c)$$

is a column vector,

$$\delta\boldsymbol{\mu}_n|_i = \mu_i - \hat{\mu}_n(z_i). \quad (3.11d)$$

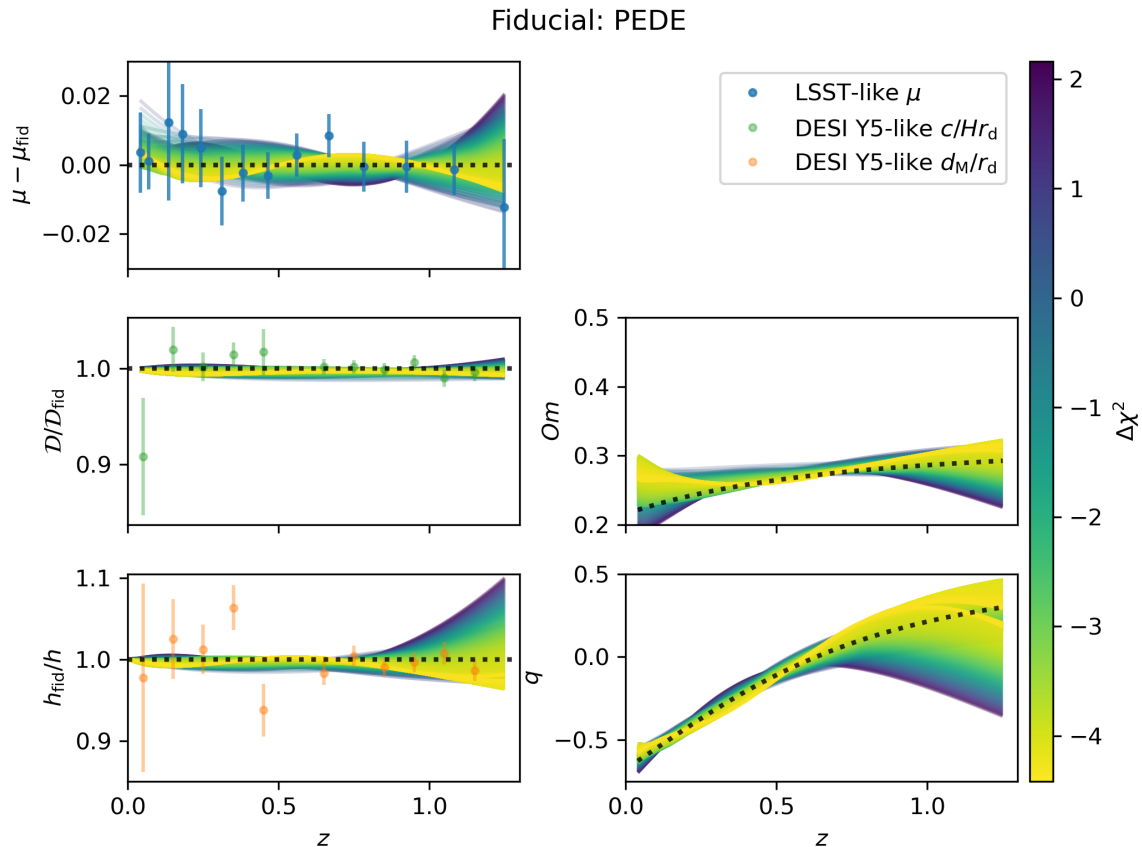


**Figure 3:** Same as Fig. 1, fiducial model: PEDE

The smoothing width is set to  $\Delta = 0.3$  following previous analyses in [39, 41–47].

We define the  $\chi^2$  value of the reconstruction  $\hat{y}_n(t)$  as

$$\chi_n^2 = \delta\boldsymbol{\mu}_n^\top \cdot \mathbf{C}_{\text{SN}}^{-1} \cdot \delta\boldsymbol{\mu}_n. \quad (3.11e)$$

The results converge towards the solution preferred by the data, independently from the choice of the initial condition [39, 41–43]. Therefore, starting from different initial conditions, the results of the iterative smoothing method will approach this solution by different paths. We collect all reconstructions with a better  $\chi^2$  than the best-fit  $\Lambda$ CDM, which then make up a non-exhaustive set of solutions.

We also obtained the smoothed first and second derivatives of  $\hat{\mu}$  as described in Appendix A. The initial guess for the derivative of the distance modulus is

$$\frac{d}{d\ln(1+z)}\hat{\mu}(z) = \frac{5}{\ln 10} \left[ 1 + \frac{1+z}{h\mathcal{D}} \sqrt{1 + \Omega_{k,0}\mathcal{D}^2} \right], \quad (3.12)$$

$$\frac{d^2}{d\ln(1+z)^2}\hat{\mu}(z) = \frac{5}{\ln 10} (1+z) \left[ \frac{\mathcal{D}'}{\mathcal{D}} \left( 1 - (1+z)\frac{\mathcal{D}'}{\mathcal{D}} \right) + (1+z)\frac{\mathcal{D}''}{\mathcal{D}} \right], \quad (3.13)$$

where  $'$  denotes  $d/dz$ . The formalism of the smooth derivative is described in the appendix.

From  $\hat{\mu}$ ,  $\hat{\mu}'$ , and  $\hat{\mu}''$ , we can reconstruct

$$\mathcal{D}(z) = \frac{H_0}{c} \frac{10^{\frac{\mu}{5}-5}}{1+z} \quad (3.14)$$

$$\mathcal{D}'(z) = \left[ \frac{\ln 10}{5} \frac{d\mu}{d \ln(1+z)} - 1 \right] \frac{\mathcal{D}(z)}{1+z}, \text{ and} \quad (3.15)$$

$$\mathcal{D}''(z) = -\frac{\mathcal{D}'}{1+z} + \left[ \frac{\ln 10}{5} \frac{d^2\mu}{d(\ln(1+z))^2} \mathcal{D} \right] + \left[ \frac{\ln 10}{5} \frac{d\mu}{d \ln(1+z)} - 1 \right] \frac{\mathcal{D}'}{1+z} \quad (3.16)$$

In practice,  $\hat{\mu}$  is reconstructed to an additive constant, and one has to normalize  $\mathcal{D}$ ,  $\mathcal{D}'$ , and  $\mathcal{D}''$  so that  $\mathcal{D}'(z=0) = 1$ .

From these relations, we can obtain  $h$ ,  $h'$ ,  $\mathcal{D}'$  via

$$\mathcal{D}' = \frac{\mathcal{D}}{1+z} \left( \frac{\ln 10}{5} \frac{d\mu}{d \ln(1+z)} - 1 \right) \quad (3.17)$$

$$h = \frac{\sqrt{1 + \Omega_{k,0} \mathcal{D}^2}}{\mathcal{D}'} \quad (3.18)$$

and

$$h' = \frac{h\mathcal{D}}{\mathcal{D}'} \left[ \frac{\Omega_{k,0}}{h^2} - \frac{\mathcal{D}''}{\mathcal{D}} \right]. \quad (3.19)$$

It is worth noting that, while we can obtain  $\mathcal{D}'$  and  $\mathcal{D}''$  from the smoothing of the supernovae directly, to obtain  $h$  and  $h'$ , one needs to know  $\Omega_{k,0}$ . Therefore, wrongly assuming flatness will imply an error when inferring  $h(z)$ ,  $h'(z)$ , and  $q(z)$ . This is just a restatement of the  $\mathcal{O}_k$  test.

## 4 Results

### 4.1 Supernova Smoothing

Fig. 1 shows the results of the smoothing for the flat- $\Lambda$ CDM model. Each line is an iteration of the smoothing color-coded by its  $\Delta\chi^2$  with respect to the best-fit  $\Lambda$ CDM model. The top-left panel shows the reconstructed distance moduli with the mock SNIa data. The middle- and bottom-left panels show the comoving distance  $\mathcal{D}(z)/\mathcal{D}_{\text{fid}}(z)$  and the expansion history  $_{\text{fid}}(z)/hh(z)$  normalized to the fiducial values. The middle- and bottom-right panels show  $O_m$  and the deceleration parameter  $q$ . We are able to reconstruct the fiducial quantities.

Figs. 2 and 3 and show the same results for the  $\Omega_{k,0} = 0.1$  and PEDE fiducial models. In the PEDE case, we are able to reconstruct the  $O_m$  and  $q$  parameters. However, it is interesting to look closely at the  $\Omega_{k,0} = 0.1$  case. Since the assumption of flatness that goes into eq. (3.3) is not true in this case, calculating  $\mathcal{D}'$  does not provide  $h$  (see eq. (3.18)). This in turn will bias our inference of  $O_m$  and  $q$  as well as the curvature test. At high-enough redshifts  $z \geq 1$ , the deviation between  $\mathcal{D}'$  and  $1/h$  becomes important. This deviation between the  $h_{\text{fid}}/h$  data from the BAO and the  $\mathcal{D}'/\mathcal{D}$  reconstructions from the SNIa are the litmus test for flatness, or signal for curvature that we are looking for. Interestingly, the reconstructions are still consistent with the fiducial  $q$ .

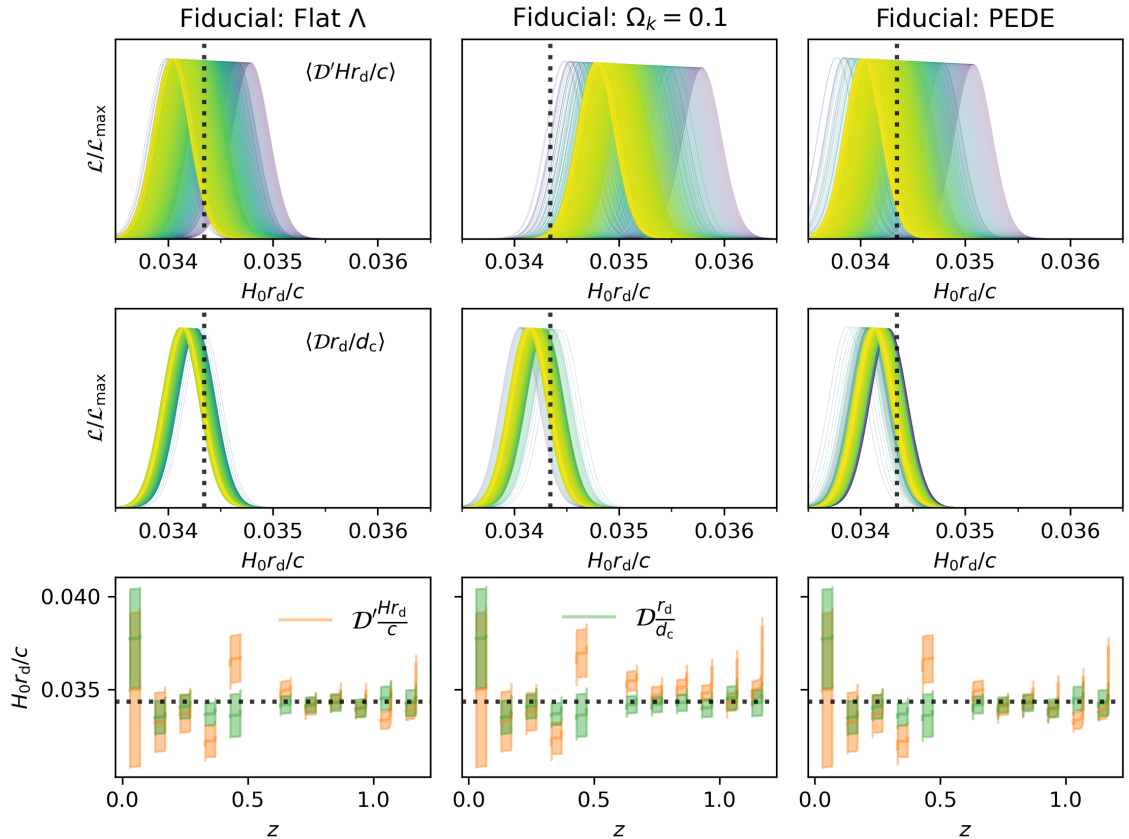


**Figure 4:** The bottom rows show our estimations of  $H_0 r_d/c$  for our two methods at the BAO data points for the three fiducial cosmologies. The central line is the collection of central values of  $H_0 r_d$  for each reconstruction, and the coloured band is the one-sigma error from the BAO around the central value. The top rows show likelihood for estimate (3.9b) at fixed iteration, and the third row for estimate (3.9a). The colour bars of the second and middle rows are the same as one of the corresponding smooth figures (1 to 2).

## 4.2 $H_0 r_d$

The bottom row of Fig. 4 shows our two estimations of  $H_0 r_d/c$  for the each model from eqs (3.9a) and (3.9b). At each BAO data point, we plot the central value and the  $\pm 1\sigma$  band for each reconstruction with  $\Delta\chi^2 = \chi^2 - \chi_{\Lambda\text{CDM}}^2 < 2.3$ . It is worth stressing here that at every BAO point, we have  $N$  estimations of  $H_0 r_d/c$ , corresponding to  $N$  reconstructions of the distance-redshift relations from the SNIa (combined with the mock BAO data point). Each of these estimates also has an associated error bar, shown as an error band on the figure. At each redshift point, the reconstructed  $H_0 r_d/c$  are re-sorted by increasing central value for aesthetic reasons. The fiducial value  $H_0 r_d^{\text{fid}}/c = 0.03435$  is shown as a dashed line. For the three fiducial cosmologies, the estimations from eq. (3.9a) are consistent with  $H_0 r_d^{\text{fid}}$ .

The top and middle rows show the likelihood of  $\Theta$  and  $\mathcal{O}_k$  for a given iteration for eq. (3.9b) and (3.9a). This is equivalent to calculating the weighted average over the different redshift bins weighted by  $1/\sigma_i^2$ . The weighted average of a quantity  $\mathbf{A} = (A(z_1), \dots, A(z_n))$

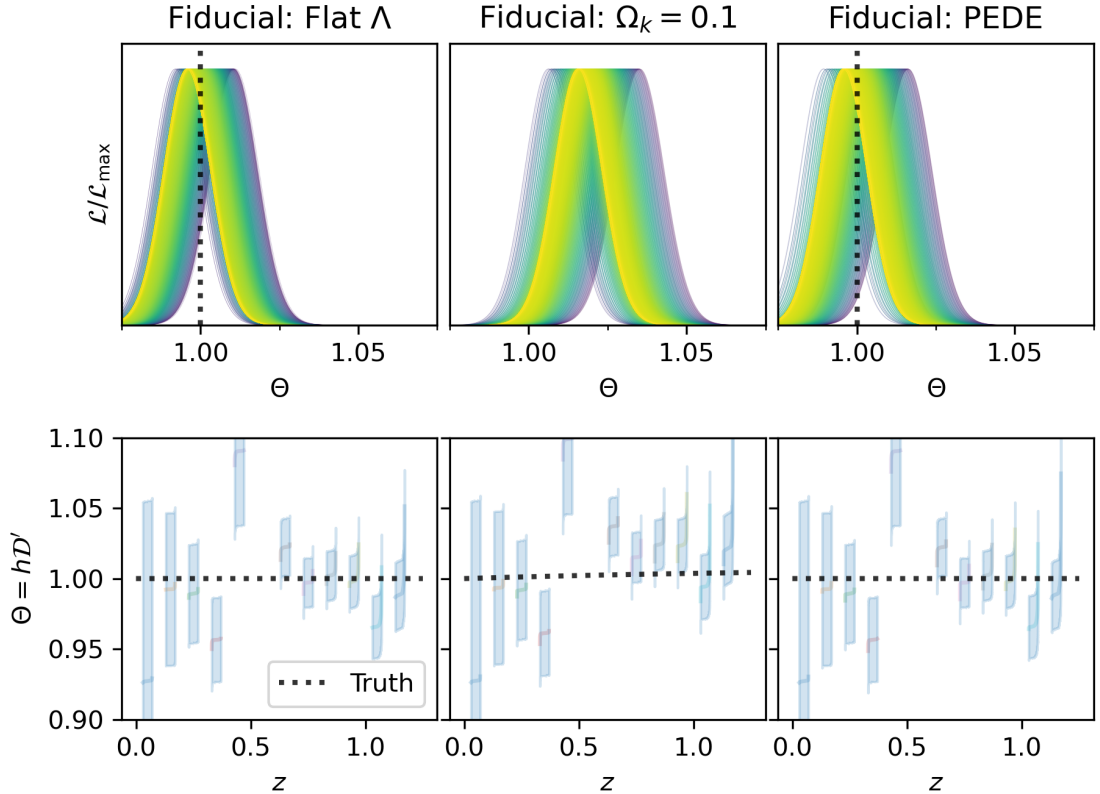


**Figure 5:** Curvature parameter:  $\Theta$ . The bottom row shows  $\Theta = h\mathcal{D}'$  for our three fiducial cosmologies. Like in Fig. 4, the central value is obtained by combining the BAO with each iteration of the smooth SN reconstructions, and the error-band from the  $1\sigma$  errors from the BAO. The top row shows the likelihood of  $\Theta$  for each smooth reconstruction. We note that in the middle panel of the top row, there is no true value for  $\Theta$  since  $\Theta(z) = \sqrt{1 + \Omega_k \mathcal{D}^2}$  varies with redshift.

with covariance matrix  $C_A$  over the different redshift bins and its variance are given by:

$$\langle A \rangle = \frac{\mathbb{1}^\top C_A^{-1} A}{\mathbb{1}^\top C_A^{-1} \mathbb{1}}, \quad (4.1a)$$

$$\sigma_{\langle A \rangle}^2 = \left( \mathbb{1}^\top C_A^{-1} \mathbb{1} \right)^{-1}. \quad (4.1b)$$

In the case of  $A = H_0 r_d$ , the correlation between two different redshift bins is negligible, and the covariance matrix in eq. (4.1) is diagonal. In the case of eq. 3.9a (middle row), the three fiducial cosmologies yield similar reconstructions, regardless of the curvature and DE. It is worth paying attention to the  $\Omega_{k,0} = 0.1$  case (middle columns). While estimator (3.9a) (third row) is totally consistent with the fiducial value, eq. (3.9b) is centred around 0.035, and most of the reconstructions are over  $2\sigma$  away from the fiducial value, showing an inconsistency between the two estimators. This comes from the fact that we do not calculate  $1/h$  but  $\mathcal{D}'$ , which do not coincide in a non-flat FLRW universe, as seen above. Indeed, we can see in the first row that the values of  $\mathcal{D}' H r_d / c$  diverge from the fiducial values at high redshift,

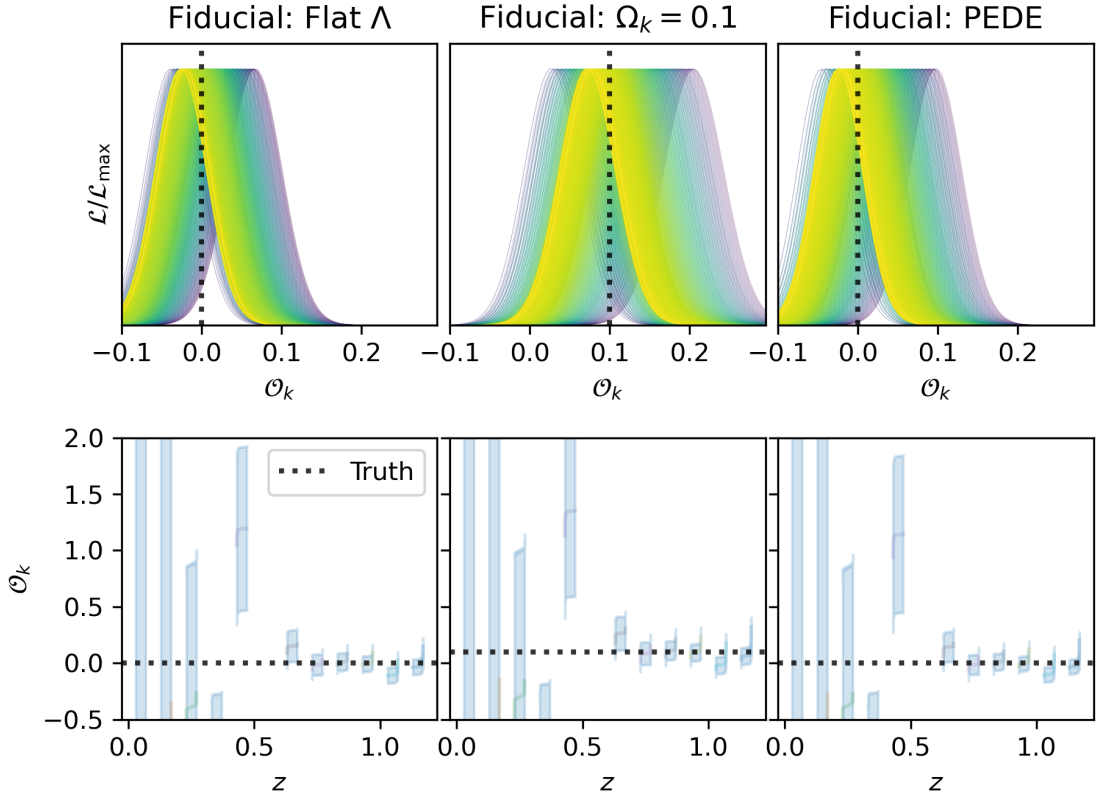


**Figure 6:** Curvature test: the  $\mathcal{O}_k$  diagnostic. Same legend as Figs. 5. The black dotted lines in the bottom row show the fiducial values of  $\Omega_{k,0}$  in all three panels,  $\Omega_{k,0} = 0$  for the left and right, and  $\Omega_{k,0} = 0.1$  for the center. It is worth noting that in the  $\Omega_{k,0} = 0.1$  case, the  $\mathcal{O}_k$  diagnostic recovers the non-zero fiducial value of  $\Omega_{k,0}$ .

Quantity	flat- $\Lambda$ CDM	$\Omega_{k,0} = 0.1$	PEDE
$\langle \mathcal{D}r_d/d_C \rangle$	0.52%	0.52%	0.52%
$\langle \mathcal{D}'Hr_d/c \rangle$	0.51%	0.51%	0.51%
$\mathcal{O}_k$	0.032–0.034	0.034–0.037	0.030–0.033
$\Theta$	0.0074–0.0075	0.0075–0.0077	0.0074–0.0076

**Table 2:** Precision for our three fiducial cosmologies. The precision for our two estimates of  $H_0r_d$  is relative to the central value, while the precisions in  $\mathcal{O}_k$  and  $\Theta$  are absolute. For  $\mathcal{O}_k$  and  $\Theta$ , we quote the minimum and maximum values. For  $H_0r_d$ , the difference between the minimum and maximum values of the precision is negligible.

reflecting equation (3.18). The minimal and maximal values of the precision of the weighted average are reported in table 2, with typically 0.5% precision.

### 4.3 Curvature Test

The Bottom panel of Fig. 5 shows our estimate of  $\Theta(z) = h\mathcal{D}' = \sqrt{1 + \Omega_{k,0}^2 \mathcal{D}}$  for the three cosmologies. The top panel shows the weighted average of  $\Theta(z)$  over  $z$  for a given iteration of the smoothing, colour-coded by  $\Delta\chi^2$  of the SNIa reconstruction. For a flat FLRW universe, we have  $\Theta(z) \equiv 1$ . Indeed, for the Flat- $\Lambda$  (left) and PEDE (right) cases, our estimates are consistent with  $\Theta = 1$ . The interesting case is the  $\Omega_{k,0} = 0.1$  case, where  $\Theta$  is not constant, and we can see a trend of  $\Theta(z)$  deviating from 1 as  $z$  increases. Similarly, the weighted average (peak of the likelihood) is larger than in the other two cases, and only marginally consistent with  $\Theta = 1$ .

Fig. 6 shows similar plots for the  $\mathcal{O}_k$  parameter. Similarly to  $\Theta$ , the Flat- $\Lambda$  and PEDE case are perfectly consistent with flatness ( $\Omega_{k,0} = 0$ ), while the  $\Omega_{k,0} = 0.1$  case is only marginally consistent with  $\Omega_{k,0} = 0$  and perfectly consistent with  $\Omega_{k,0} = 0.1$ , showing the constraining power of this test.

In the bottom panels of both figures, at  $z \gtrsim 0.5$ , the error bars are very small and the reconstructions are perfectly consistent with the fiducial cosmology in all three cases. At low redshift, the large error bars do not constrain  $\Theta$  or  $\Omega_{k,0}$ .

## 5 Summary and Conclusion

We combined forecast BAO data for a DESI 5-year-like survey and a realistic forecast for LSST SNIa to assess the ability of the joint surveys to provide model-independent litmus tests of the flat  $\Lambda$ CDM model. For this purpose, we generated mock data for three cosmologies: flat  $\Lambda$ CDM a non-flat  $\Lambda$ CDM universe with  $\Omega_{k,0} = 0.1$ , and an example of dynamical dark energy, the PEDE model.

We applied the iterative smoothing method to reconstruct the expansion history in a model-independent manner, only assuming flatness.

The expected quality of LSST SNIa will allow to reconstruct very accurately certain diagnostics such as  $Om$  and  $q$ . In addition, we quantify the ability of the joint surveys to constrain  $H_0 r_d/c$ . We then proceed to testing the FLRW metric, measuring  $\Theta$  and  $\mathcal{O}_k$ . The combination of LSST and DESI 5-years will allow to constrain  $\mathcal{O}_k$  to within  $\sim 0.035$ , and  $\Theta$  to within 0.0075. It is worth noting that the credible interval reported by DESI DR1 is  $(-0.078, 0.068)$  for the flat  $\Lambda$ CDM model without any external data. We show that with the expected five-year data accuracy, a model-independent precision on the curvature parameter will be competitive.

In the case of the  $\Omega_{k,0} = 0.1$  universe, the flatness assumption of eq. (3.3) is now incorrect, which leads to a biased expansion history and inconsistent estimations of  $H_0 r_d/c$  from our two methods. Therefore,  $H_0 r_d$  itself can be seen as a curvature test. An inconsistency between the two estimates of  $H_0 r_d$ , or with  $\mathcal{O}_k(z) = 1$  or  $\Theta(z) = 1$  can just be interpreted either as evidence of departure from flatness, or inconsistency between the two data sets.

## A Smooth Derivatives

An interesting property of smoothing is that the derivative of the smooth function can be readily obtained from the derivative of the smoothing kernel.

Suppose we observe a function  $y_i = f(t) + \epsilon_i$ , where  $\epsilon \sim \mathcal{N}(0, \mathbf{C})$ . We want to reconstruct the smooth function  $\hat{f}(t)$  and its successive derivative  $\hat{f}^{(i)}(t)$ .

$$\hat{y}_{n+1}(t) = \hat{y}_n(t) + \frac{\boldsymbol{\delta y}_n^\top \cdot \mathbf{C}^{-1} \cdot \mathbf{W}(t)}{\mathbb{1}^\top \cdot \mathbf{C}^{-1} \cdot \mathbf{W}(t)}, \quad (\text{A.1})$$

where  $\mathbb{1}^\top = (1, \dots, 1)$ , the weight  $\mathbf{W}$  and residual  $\boldsymbol{\delta y}_n$  denote

$$W_i(t) = \exp \left[ -\frac{(t - t_i)^2}{2\Delta^2} \right] \quad (\text{A.2})$$

$$\boldsymbol{\delta y}_n|_i = y_i - \hat{y}_n(t_i) \quad (\text{A.3})$$

and  $\mathbf{C}^{-1}$  indicates the inverse of covariance matrix of the data. The smoothing width is set to  $\Delta = 0.3$  as mentioned in eq. (3.11).

Since smoothing is essentially a convolution by a smoothing kernel, one can straightforwardly define the smooth reconstruction of the successive derivatives as

$$\hat{y}_{n+1}(t) = \hat{y}_n(t) + \frac{B(t)}{A(t)}, \quad (\text{A.4})$$

where

$$B = \boldsymbol{\delta y}_n \cdot \mathbf{C}^{-1} \cdot \mathbf{W}(t), \text{ and} \quad (\text{A.5})$$

$$A = \mathbb{1}^\top \cdot \mathbf{C}^{-1} \cdot \mathbf{W}(t). \quad (\text{A.6})$$

The first and second smooth derivatives is obtained by deriving the previous equation with respect to  $t$ :

$$\hat{y}'_{n+1}(t) = \hat{y}'_n(t) + \frac{B'}{A} - \frac{BA'}{A^2}, \quad (\text{A.7})$$

$$\hat{y}''_{n+1}(t) = \hat{y}''_n(t) + \frac{B''}{A} - \frac{2A'B' + A''B}{A^2} + \frac{2A'^2B}{A^3}, \quad (\text{A.8})$$

where

$$B' = \boldsymbol{\delta y}_n^\top \cdot \mathbf{C}^{-1} \cdot \mathbf{W}'(t), \quad (\text{A.9})$$

$$A' = \mathbb{1}^\top \cdot \mathbf{C}^{-1} \cdot \mathbf{W}'(t), \quad (\text{A.10})$$

$$B'' = \boldsymbol{\delta y}_n^\top \cdot \mathbf{C}^{-1} \cdot \mathbf{W}''(t), \text{ and} \quad (\text{A.11})$$

$$A'' = \mathbb{1}^\top \cdot \mathbf{C}^{-1} \cdot \mathbf{W}''(t). \quad (\text{A.12})$$

In this work, we apply the algorithm to the LSST simulated SNIa with  $t = \ln(1 + z)$ .

## Acknowledgments

B. L. acknowledges the support of the National Research Foundation of Korea (NRF-2022R1F1A1076338 and RS-2023-00259422). AM thanks Richard Kessler and the LSST DESC TD team for the production of the LSST dataset.

## References

- [1] PLANCK collaboration, Planck 2018 results. VI. Cosmological parameters, *Astron. Astrophys.* **641** (2020) A6.
- [2] D.J. Eisenstein, I. Zehavi, D.W. Hogg, R. Scoccimarro, M.R. Blanton, R.C. Nichol et al., *Detection of the Baryon Acoustic Peak in the Large-Scale Correlation Function of SDSS Luminous Red Galaxies*, *ApJ* **633** (2005) 560 [[astro-ph/0501171](#)].
- [3] S. Alam, M. Aubert, S. Avila et al., *Completed SDSS-IV extended Baryon Oscillation Spectroscopic Survey: Cosmological implications from two decades of spectroscopic surveys at the Apache Point Observatory*, *Phys. Rev. D* **103** (2021) 083533 [[2007.08991](#)].
- [4] DESI Collaboration, A.G. Adame et al., *DESI 2024 IV: Baryon Acoustic Oscillations from the Lyman Alpha Forest*, *arXiv e-prints* (2024) [[2404.03001](#)].
- [5] DESI Collaboration, A.G. Adame et al., *DESI 2024 VI: Cosmological Constraints from the Measurements of Baryon Acoustic Oscillations*, *arXiv e-prints* (2024) [[2404.03002](#)].
- [6] DESI Collaboration, A.G. Adame et al., *DESI 2024 III: Baryon Acoustic Oscillations from Galaxies and Quasars*, *arXiv e-prints* (2024) [[2404.03000](#)].
- [7] S. Perlmutter, G. Aldering, G. Goldhaber, R.A. Knop, P. Nugent et al., *Measurements of  $\Omega$  and  $\Lambda$  from 42 High-Redshift Supernovae*, *Astrophys. J.* **517** (1999) 565 [[astro-ph/9812133](#)].
- [8] A.G. Riess, A.V. Filippenko, P. Challis, A. Clocchiatti, A. Diercks et al., *Observational Evidence from Supernovae for an Accelerating Universe and a Cosmological Constant* [[arXiv:astro-ph/9805201](#)], *Astron. J.* **116** (1998) 1009 [[astro-ph/9805201](#)].
- [9] M. Betoule et al., *Improved cosmological constraints from a joint analysis of the SDSS-II and SNLS supernova samples*, *Astron. Astrophys.* **568** (2014) A22 [[1401.4064](#)].
- [10] PAN-STARRS1 collaboration, *The Complete Light-curve Sample of Spectroscopically Confirmed SNe Ia from Pan-STARRS1 and Cosmological Constraints from the Combined Pantheon Sample*, *Astrophys. J.* **859** (2018) 101.
- [11] D. Brout et al., *The Pantheon+ Analysis: Cosmological Constraints*, *Astrophys. J.* **938** (2022) 110 [[2202.04077](#)].
- [12] R.E. Keeley, A. Shafieloo, G.-B. Zhao, J.A. Vazquez and H. Koo, *Reconstructing the Universe: Testing the Mutual Consistency of the Pantheon and SDSS/eBOSS BAO Data Sets with Gaussian Processes*, *AJ* **161** (2021) 151 [[2010.03234](#)].
- [13] S.-g. Hwang, B. L’Huillier, R.E. Keeley, M.J. Jee and A. Shafieloo, *How to use GP: effects of the mean function and hyperparameter selection on Gaussian process regression*, *J. Cosmology Astropart. Phys.* **2023** (2023) 014 [[2206.15081](#)].
- [14] R.E. Keeley and A. Shafieloo, *Ruling Out New Physics at Low Redshift as a Solution to the  $H_0$  Tension*, *Phys. Rev. Lett.* **131** (2023) 111002 [[2206.08440](#)].
- [15] P.K. Aluri et al., *Is the observable Universe consistent with the cosmological principle?*, *Class. Quant. Grav.* **40** (2023) 094001 [[2207.05765](#)].
- [16] L. Perivolaropoulos and F. Skara, *Challenges for  $\Lambda$ CDM: An update*, *New Astron. Rev.* **95** (2022) 101659 [[2105.05208](#)].
- [17] M. Kamionkowski and A.G. Riess, *The Hubble Tension and Early Dark Energy*, [2211.04492](#).
- [18] E. Di Valentino, O. Mena, S. Pan, L. Visinelli, W. Yang, A. Melchiorri et al., *In the realm of the Hubble tension—a review of solutions*, *Class. Quant. Grav.* **38** (2021) 153001 [[2103.01183](#)].
- [19] C. Krishnan, R. Mohayaee, E.O. Colgáin, M.M. Sheikh-Jabbari and L. Yin, *Does Hubble tension signal a breakdown in FLRW cosmology?*, *Class. Quant. Grav.* **38** (2021) 184001 [[2105.09790](#)].

- [20] E. Abdalla et al., *Cosmology intertwined: A review of the particle physics, astrophysics, and cosmology associated with the cosmological tensions and anomalies*, *JHEAp* **34** (2022) 49 [2203.06142].
- [21] C. Krishnan, R. Mohayaee, E.O. Colgáin, M.M. Sheikh-Jabbari and L. Yin, *Hints of FLRW breakdown from supernovae*, *Phys. Rev. D* **105** (2022) 063514 [2106.02532].
- [22] T.L. Smith, M. Lucca, V. Poulin, G.F. Abellan, L. Balkenhol, K. Benabed et al., *Hints of early dark energy in Planck, SPT, and ACT data: New physics or systematics?*, *Phys. Rev. D* **106** (2022) 043526 [2202.09379].
- [23] J. Sola Peracaula, *The cosmological constant problem and running vacuum in the expanding universe*, *Phil. Trans. Roy. Soc. Lond. A* **380** (2022) 20210182 [2203.13757].
- [24] K. Lodha, A. Shafieloo, R. Calderon, E. Linder, W. Sohn, J.L. Cervantes-Cota et al., *DESI 2024: Constraints on Physics-Focused Aspects of Dark Energy using DESI DR1 BAO Data*, *arXiv e-prints* (2024) arXiv:2405.13588 [2405.13588].
- [25] R. Calderon, K. Lodha, A. Shafieloo, E. Linder, W. Sohn, A. de Mattia et al., *DESI 2024: Reconstructing Dark Energy using Crossing Statistics with DESI DR1 BAO data*, *arXiv e-prints* (2024) arXiv:2405.04216 [2405.04216].
- [26] E. Di Valentino, A. Melchiorri and J. Silk, *Cosmological constraints in extended parameter space from the Planck 2018 Legacy release*, *J. Cosmology Astropart. Phys.* **2020** (2020) 013 [1908.01391].
- [27] DESI Collaboration, A. Aghamousa et al., *The DESI Experiment Part I: Science, Targeting, and Survey Design*, *arXiv e-prints* (2016) arXiv:1611.00036 [1611.00036].
- [28] X. Li and A. Shafieloo, *A Simple Phenomenological Emergent Dark Energy Model can Resolve the Hubble Tension*, *ApJ* **883** (2019) L3 [1906.08275].
- [29] LSST DARK ENERGY SCIENCE collaboration, *Using Host Galaxy Photometric Redshifts to Improve Cosmological Constraints with Type Ia Supernovae in the LSST Era*, *Astrophys. J.* **944** (2023) 212 [2210.07560].
- [30] LSST collaboration, *LSST: from Science Drivers to Reference Design and Anticipated Data Products*, *Astrophys. J.* **873** (2019) 111 [0805.2366].
- [31] R. Kessler, J.P. Bernstein, D. Cinabro, B. Dilday, J.A. Frieman, S. Jha et al., *SNANA: A Public Software Package for Supernova Analysis*, *Publ. Astron. Soc. Pac.* **121** (2009) 1028 [0908.4280].
- [32] THE PLASSTICC TEAM collaboration, *The Photometric LSST Astronomical Time-series Classification Challenge (PLASSTICC): Data set*, *arXiv:1810.00001* (2018) .
- [33] R.S. de Jong, O. Agertz, A.A. Berbel, J. Aird, D.A. Alexander et al., *4MOST: Project overview and information for the First Call for Proposals*, *The Messenger* **175** (2019) 3 [1903.02464].
- [34] R. Kessler, D. Cinabro, B. Bassett, B. Dilday, J.A. Frieman et al., *Photometric Estimates of Redshifts and Distance Moduli for Type Ia Supernovae*, *Astrophys. J.* **717** (2010) 40 [1001.0738].
- [35] M.L. Graham, A.J. Connolly, Ž. Ivezić, S.J. Schmidt, R.L. Jones, M. Jurić et al., *Photometric Redshifts with the LSST: Evaluating Survey Observing Strategies*, *Astron. J.* **155** (2018) 1 [1706.09507].
- [36] LSST DARK ENERGY SCIENCE collaboration, *The LSST Dark Energy Science Collaboration (DESC) Science Requirements Document*, *arXiv:1809.01669* (2018) [1809.01669].
- [37] C. Clarkson, B. Bassett and T.H.-C. Lu, *A General Test of the Copernican Principle*, *Physical Review Letters* **101** (2008) 011301 [0712.3457].

- [38] A. Shafieloo and C. Clarkson, *Model independent tests of the standard cosmological model*, *Phys. Rev. D* **81** (2010) 083537 [[0911.4858](#)].
- [39] B. L’Huillier and A. Shafieloo, *Model-independent test of the FLRW metric, the flatness of the Universe, and non-local estimation of  $H_0$   $r_d$* , *J. Cosmology Astropart. Phys.* **2017** (2017) 015 [[1606.06832](#)].
- [40] V. Sahni, A. Shafieloo and A.A. Starobinsky, *Two new diagnostics of dark energy*, *Phys. Rev. D* **78** (2008) 103502 [[0807.3548](#)].
- [41] A. Shafieloo, U. Alam, V. Sahni and A.A. Starobinsky, *Smoothing supernova data to reconstruct the expansion history of the Universe and its age*, *MNRAS* **366** (2006) 1081 [[astro-ph/0505329](#)].
- [42] A. Shafieloo, *Model-independent reconstruction of the expansion history of the Universe and the properties of dark energy*, *MNRAS* **380** (2007) 1573 [[astro-ph/0703034](#)].
- [43] A. Shafieloo, B. L’Huillier and A.A. Starobinsky, *Falsifying  $\Lambda$ CDM : Model-independent tests of the concordance model with eBOSS DR14Q and Pantheon*, *Phys. Rev. D* **98** (2018) 083526 [[1804.04320](#)].
- [44] B. L’Huillier, A. Shafieloo and H. Kim, *Model-independent cosmological constraints from growth and expansion*, *MNRAS* **476** (2018) 3263 [[1712.04865](#)].
- [45] H. Koo, A. Shafieloo, R.E. Keeley and B. L’Huillier, *Model-independent Constraints on Type Ia Supernova Light-curve Hyperparameters and Reconstructions of the Expansion History of the Universe*, *ApJ* **899** (2020) 9 [[2001.10887](#)].
- [46] H. Koo, A. Shafieloo, R.E. Keeley and B. L’Huillier, *Model selection and parameter estimation using the iterative smoothing method*, *J. Cosmology Astropart. Phys.* **2021** (2021) 034 [[2009.12045](#)].
- [47] H. Koo, R.E. Keeley, A. Shafieloo and B. L’Huillier, *Bayesian vs frequentist: comparing Bayesian model selection with a frequentist approach using the iterative smoothing method*, *J. Cosmology Astropart. Phys.* **2022** (2022) 047 [[2110.10977](#)].